Experimental and computational diagnosis of the fluxional nature of a benzene-1,3,5-tricarboxamide-based hydrogen-bonded dimer

Matthieu Raynal, Yan Li, Claire Troufflard, Cédric Przybylski, Geoffrey Gontard, Thomas Maistriaux, Julien Idé, Roberto Lazzaroni, Laurent Bouteiller, Patrick Brocorens

PCCP
Physical Chemistry Chemical Physics

Accepted Manuscript

This article can be cited before page numbers have been issued, to do this please use: M. Raynal, Y. Li, C. Troufflard, C. Przybylski, G. Gontard, T. Maistriaux, J. Idé, R. Lazzaroni, L. Bouteiller and P. Brocorens, *Phys. Chem. Chem. Phys.*, 2021, DOI: 10.1039/D0CP06128J.

ROYAL SOCIETY OF CHEMISTRY

rsc.li/pccp

View Article Online
DOI: 10.1039/D0CP06128J

ARTICLE

Experimental and computational diagnosis of the fluxional nature of a benzene-1,3,5-tricarboxamide-based hydrogen-bonded dimer

Received 00th January 20xx,
Accepted 00th January 20xx

DOI: 10.1039/x0xx00000x

M. Raynal,*[a] Y. Li,[a] C. Troufflard,[a] C. Przybylski,[a] G. Gontard,[a] T. Maistriaux,[b] J. Idé,[b] R. Lazzaroni,[b] L. Bouteiller,[a] and P. Brocorens*[b]

Precise characterization of the hydrogen bond network present in discrete self-assemblies of benzene-1,3,5-tricarboxamide monomers derived from amino-esters (ester BTAs) is crucial for the construction of elaborated functional co-assemblies. For all ester BTA dimeric structures previously reported, ester carbonyls in the side chain act as hydrogen bond acceptors, yielding well-defined dimers stabilized by six hydrogen bonds. The ester BTA monomer derived from glycine (**BTA Gly**) shows a markedly different self-assembly behaviour. We report herein a combined experimental and computational investigation aimed at determining the nature of the dimeric species formed by **BTA Gly**. Two distinct dimeric structures were characterized by single crystal X-Ray diffraction measurements. Likewise, a range of spectroscopic and scattering techniques as well as molecular modelling were employed to diagnose the nature of the dynamic dimeric structures in toluene. Our results unambigously establish that both ester and amide carbonyls are involved in the hydrogen bond network of the discrete dimeric species formed by **BTA Gly**. The participitation of roughly 4.5 ester carbonyls and 1.5 amide carbonyls per monomer as determined by FT-IR spectroscopy implies that several conformations coexist in solution. Moreover, NMR analysis and modelling data reveal rapid interconversion between these different conformers leading to a symmetric structure on the NMR timescale. Rapid hydrogen bond shuffling between conformers having three (three), two (four), one (five) and zero (six) amide carbonyl group (ester carbonyl respectively) as hydrogen bond acceptors is proposed to explain the magnetic equivalence of the amide N−H on the NMR timescale. When compared to other ester BTA derivatives for which only ester carbonyls are acting as hydrogen bonding acceptors, the fluxional behaviour of the hydrogen-bonded dimers of **BTA Gly** likely originates from a larger range of energetically-favorable conformations accessible through rotation of the BTA side chains.

Introduction

The self-assembly of small complementary monomers through non-covalent interactions can generate intricate and functional nanostructures in an expeditious manner.[1-4] Dynamic helical polymers are thus usually obtained through aggregation of structurally simple disk-like monomers through a combination of hydrogen bonding and aromatic interactions.[5-9] *N*,*N*',*N*''-Trialkyl benzene-1,3,5-tricarboxamides (alkyl BTAs) are prominent members of this family.[10] Upon stacking, alkyl BTA monomers generate helical rod-like assemblies with a relatively rigid central core because of the strongly-connected amide functions and interacting aromatic rings. This core is surrounded by protruding alkyl chains that are inherently more flexible (see a representation in Chart 1a). A range of spectroscopic and scattering techniques has unambiguously established that similar helical assemblies are present in liquid crystals,[11-13] in single crystals,[14, 15] in dilute solutions[16-19] and in gels.[20-22] Introduction of functional groups at the periphery of BTA assemblies is required to favour their formation in water,[23-29] their hybridization with oligonucleotides,[30-32] or their implementation as catalysts,[33-42] circularly-polarized light emitters[43] or luminescent gels.[44] Moreover, mixing different types of BTA monomers has recently emerged as a remarkable method to control the chirality and structure of helical co-assemblies[45-48] and construct elaborate functional supramolecular materials.[37-39, 41, 49]

Deriving BTA monomers by grafting α-amino esters (ester BTAs, Chart 1b)[50-62] is an appealing strategy to modulate the nature of groups and functions attached to the amide functions. Previous studies have revealed that the nature of the self-assemblies formed by ester BTAs is strongly dependent on the nature and stereochemistry of the group (R^1 in Chart 1b) located next to the amide function as well as on experimental conditions.[57-59] The involvement of ester carbonyls as hydrogen bond (HB) acceptors increases the range of possible structures, making it difficult to rationalize which one(s) is(are) the most stable.[63] Our previous systematic study[58] of association properties in dilute solutions and gels led us to rank ester BTA monomers into three main categories,

[a] *Sorbonne Université, CNRS, IPCM, UMR 8232, 4 Place Jussieu, 75252 Paris cedex 05, France. E-mail : matthieu.raynal@sorbonne-universite.fr.*
[b] *Service de Chimie des Matériaux Nouveaux, Institut de Recherche sur les Matériaux, Université de Mons, Place du Parc, 20, B-7000, Mons, Belgium. E-mail : patrick.brocorens@umons.ac.be.*

†Electronic Supplementary Information (ESI) available: Chart S1, Tables S1-S14, Figures S1-S11, additional experimental and computational data. See DOI: 10.1039/x0xx00000x

View Article Online
DOI: 10.1039/D0CP06128J

ARTICLE

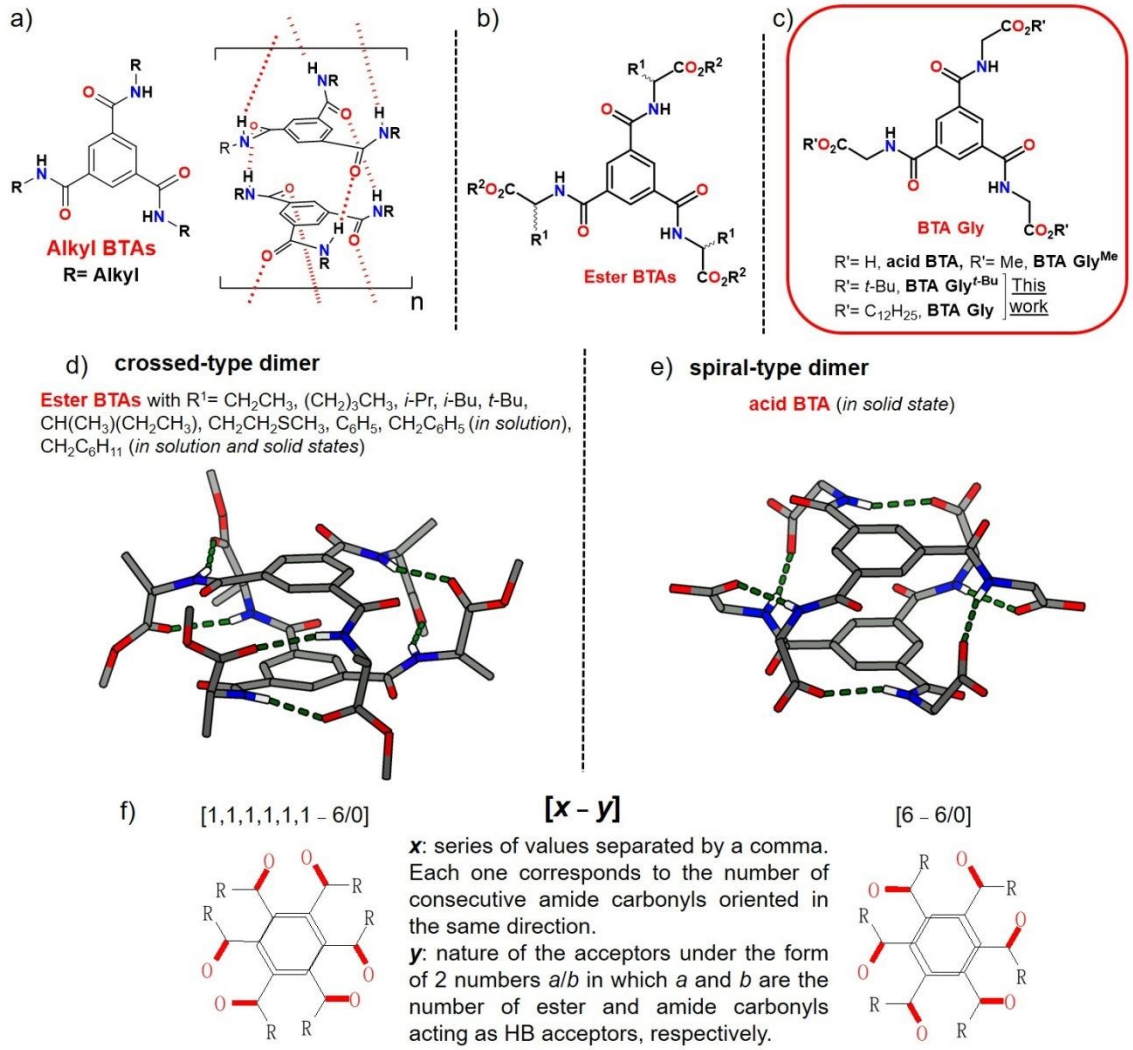

Chart 1. a) Chemical structures of alkyl BTA and schematic representation of their stacking arrangement into helical rod-like assemblies. b) Chemical structure of ester BTAs. c) Chemical structures of **BTA Gly** monomers. d) « Sticks » representation of the crossed-type dimeric structure (adapted from the X-ray structure of the ester BTA for which R^1= $CH_2C_6H_{11}$).[59] e) « Sticks » representation of the spiral-type dimeric structure (adapted from the X-ray structure of **acid BTA**). Water molecules connected to amide carbonyls and to the OH group of the acid functions are not shown.[64] f) Nomenclature adopted throughout this paper to describe the different conformers, and simplified representation of the crossed-type and spiral-type BTA dimers to show the relative orientation (as observed perpendicularly to the aromatic rings) of the amide carbonyl groups (highlighted in red). Left: the orientation of the amide carbonyls alternates from one branch to the next and all hydrogen bonded carbonyls are esters, hence the name [1,1,1,1,1,1 - 6/0]. Right: all six amide carbonyls are oriented in the same way (here as a 'counter clockwise windmill') and all hydrogen bonded carbonyls are esters, hence the name [6 - 6/0].

depending on the self-assemblies they form: dimers only, stacks only, or both structures in competition. Alternatively helical stacks are the most common structures in liquid crystals and crystals, even though other hydrogen-bonded arrangements might also form.[54, 55, 58-60, 65]

A range of analytical data, including X-ray analyses on single crystals,[59] as well as modelling studies have unambiguously ascertained the nature of the dimers formed by the ester BTAs listed in Chart 1d.[58] Two BTA monomers are stacked in such a way that the six arms are connected pairwise through reciprocal hydrogen bonds between the amide N–H and the ester carbonyls (Chart 1d). Those crossed-type dimers proved to be highly stable in solution, probably because of the six-fold hydrogen bonds connecting the BTA monomers. Remarkably, no reorganization of the hydrogen bond network, *i.e.*

involvement of the amide carbonyl, was detected upon high dilution or heating.

Contrariwise, our initial studies failed to identify the nature of the self-assemblies formed by the ester BTA derived from the dodecyl ester of Glycine (**BTA Gly**, Chart 1c). In our quest for a potential structure of this structurally simple ester BTA, we noted that a BTA directly derived from Glycine (**acid BTA**, Chart 1c) had been found to adopt a dimeric structure involving carbonyls of the carboxyl groups as HB acceptors but with a very different HB pattern from that of the crossed-type dimers. Indeed, each arm is bonded to the next one by only one hydrogen bond, thus forming spiral-type dimers (Chart 1e).[64] However, it remains an open question whether this type of dimer exists as isolated species in solution. In the present study, the nature of the species formed by **BTA Gly** and **BTA Gly$^{t\text{-Bu}}$** (Chart 1c) in the crystalline state and in solution has been characterized by a combination of experimental techniques and computational methods. Our studies reveal that several conformers of **BTA Gly** are energetically accessible leading to several polymorphs in solid state and a mixture of species in solution. These discrete dimeric species are highly fluxional because of the rapid exchange between the HB acceptors, ester and amide carbonyls, engaged in the hydrogen bond network.

Experimental and computational details

Synthetic procedures

The synthesis and characterization of **BTA Gly** has been described previously.[58] The detailed synthesis of **BTA Gly$^{t\text{-Bu}}$** is described in the ESI.† *tert*-butyl glycinate was synthesized according to a published procedure[66] and isolated as its HCl salt. Benzene-1,3,5-tricarbonyl trichloride was purchased from Alfa Aesar. Dry CH_2Cl_2 was obtained from an SPS solvent purification system (IT-Inc). NMR spectra were recorded on a Bruker Avance 300 spectrometer and calibrated to the residual solvent peak of acetone-d_6 (^{1}H: 2.05 ppm; ^{13}C: 29.84 ppm). Peaks are reported with their corresponding multiplicity (s: singlet; d: doublet, t: triplet) and integration, and respective *J* coupling constants are given in Hertz. High-resolution mass spectrometry (HRMS) measurements were obtained on LTQ-Orbitrap XL-ETD by electrospray ionization in positive mode. FT-IR spectra for solids were recorded by reflection on a Ge probe (attenuated total reflectance (ATR)). The main bands were reported as w: weak, m: medium, s: strong, br: broad, sh: shoulder.

X-Ray crystal structure determination

A single crystal was selected, mounted, and transferred into a cold nitrogen gas stream. Intensity data were collected with a Bruker Kappa-APEX2 system using micro-source Cu-Kα radiation. Unit-cell parameters determination, data collection strategy, integration and absorption correction were carried out with the Bruker APEX2 suite of programs. The structure was solved with SHELXT[67] and refined anisotropically by full-matrix least-squares methods with SHELXL[67] using the WinGX suite. Structures were deposited at the Cambridge Crystallographic Data Centre with numbers CCDC 2015081 and CCDC 2015082 and can be obtained free of charge via www.ccdc.cam.ac.uk.

Crystal data for **BTA Gly$^{t\text{-Bu}}$** (spiral-type dimer, [6 – 6/0]). $C_{27}H_{39}N_3O_9$, cubic P a-3, a = b = c = 18.2873(3) Å, α = β = γ = 90°, V = 6115.7(3) Å^3, Z = 8, colorless prism 0.25 × 0.2 × 0.1 mm^3, μ = 0.747 mm^{-1}, min / max transmission = 0.81 / 0.92, T= 200(1) K, λ = 1.54178 Å, θ range = 4.84° to 66.60°, 16564 reflections measured, 1813 independent, R_{int} = 0.0641, completeness = 0.999, 119 parameters, 0 restraints, final R indices R1 [I>2σ(I)] = 0.0406 and wR2 (all data) = 0.1098, GOF on F^2 = 1.031, largest difference peak / hole = 0.21 / -0.20 e·Å^{-3}.

Crystal data for **BTA Gly$^{t\text{-Bu}}$** (dissymmetric dimer, [4,2 – 2/2]). $C_{27}H_{39}N_3O_9$, monoclinic P 2_1/c, a = 13.6976(2) Å, b = 15.5866(3) Å, c = 28.4803(5) Å, α = γ = 90°, β = 91.1670(10)°, V = 6079.25(18) Å^3, Z = 8, colorless prism 0.3 × 0.2 × 0.05 mm^3, μ = 0.751 mm^{-1}, min / max transmission = 0.83 / 0.98, T= 170(1) K, λ = 1.54178 Å, θ range = 3.23° to 66.64°, 52508 reflections measured, 10742 independent, R_{int} = 0.0570, completeness = 0.999, 703 parameters, 0 restraints, final R indices R1 [I>2σ(I)] = 0.0550 and wR2 (all data) = 0.1565, GOF on F^2 = 1.037, largest difference peak / hole = 0.81 / -0.44 e·Å^{-3}.

Fourier-Transform Infrared (FT-IR) analyses

FT-IR measurements were performed on a Nicolet iS10 spectrometer. Spectra of solutions of **BTA Gly** and **BTA Gly$^{t\text{-Bu}}$** in toluene were measured at 293 K in CaF_2 cells with 0.05 cm (1 mM – 25 mM), 0.01 cm (50 mM) or 0.005 cm (100 and 200 mM) path length and were corrected for air, toluene and cell absorption. The FT-IR spectrum of crystals of **BTA Gly$^{t\text{-Bu}}$** was recorded by reflection on a Ge probe (ATR-FTIR). For variable-temperature (VT) FT-IR measurements of **BTA Gly** (1 mM), the temperature was controlled with a digital temperature controller (West 6100+) from Specac and the spectra were recorded in a KBr cell (path length of 0.1 cm). Full spectra were measured every 10°C (heating rate: 1°C.min^{-1}) between 30°C and 100°C. The data were not corrected for the thermal expansion of the solutions.

Small-angle neutron scattering (SANS) analyses

SANS measurements were made at the Laboratoire Louis Brillouin (Saclay, France) on the PA20 instrument, at two distance-wavelength combinations to cover the 5.6×10^{-3} to 0.46 Å^{-1} *q*-range, where the scattering vector q is defined as usual, assuming elastic scattering, as $q=(4\pi/\lambda)\sin(\theta/2)$, where θ is the angle between incident and scattered beam. The data were corrected for the empty cell signal and the solute and solvent incoherent background. A light water standard was used to normalize the scattered intensities to cm^{-1} units. The data were fitted with the DANSE software SasView.

High-Resolution Mass Spectroscopy (HRMS)

Electrospray-high resolution mass spectrometry (ESI-HRMS) analysis of **BTA Gly** and **BTA Gly$^{t\text{-Bu}}$** samples were made at 1 μg.ml^{-1} in acetonitrile/toluene 25/75. Experiments were carried out using a LTQ-Orbitrap XL-ETD mass spectrometer (Thermo Scientific, San Jose, CA, USA) operated in positive ionization mode with a spray voltage at 3.6 kV. Sample was continuously infused using a 250 μL syringe at a flow rate of 3

µL.min^{-1}. Applied voltages were 40 and 100 V for the ion transfer capillary and the tube lens, respectively. The ion transfer capillary was held at 275°C. No sheath or auxiliary gas was used. Detection was achieved in the Orbitrap with a resolution set to 100,000 (at m/z 400) and a m/z range between 200-2000 (normal range setting) in profile mode. Spectra were analysed using the acquisition software XCalibur 2.1 (Thermo Fisher Scientific, Courtaboeuf, France) without smoothing and background subtraction. An automatic gain control allowed accumulation of up to 2.10^5 for FTMS scans. Maximum injection time was set to 500 with 1 µscan.

NMR spectroscopy

^{1}H NMR experiments were recorded at 300 K on a Bruker Avance I 400 spectrometer (9.4 T) equipped with an observe broadband probe. All spectra were acquired in 5 mm NMR tubes. Each NMR tube contained *ca.* 10 mM of **BTA Gly** in C_7D_8 (^{1}H: 2.08 ppm). Variable-temperature (VT) ^{1}H NMR experiments were conducted as follows: The first ^{1}H NMR experiment was recorded at 300 K in order to ensure a good homogeneity of the shims. Then, the rotating sample was cooled slowly stepwise to avoid degrading the quality of the shims thanks to a liquid nitrogen exchanger connected to the probe. The ^{1}H NMR acquisition at 223K was started 15 minutes after reaching this temperature. 2D-homonuclear experiments (COSY and ROESY) were performed on a Bruker Avance III 600 spectrometer (14.1T) at 300 K equipped with an observe broadband probe. All spectra were acquired in 5 mm NMR tubes.

Molecular modelling

Dimers of **BTA Gly** were built and computed with the Materials Studio 6.0 modelling package.[68] To alleviate the computational cost, the dodecyl chains were replaced by methyls, and no explicit solvent was used. Both approximations are reasonable as, on one side, the alkyl chains do not appear critical in the formation of dimers in solution (both molecules substituted by the long dodecyl and by the short and bulky t-Bu chains have the same experimental infrared spectra, see Figure S2a), and on the other side, the assemblies are mainly driven by the six hydrogen bonds, and the aprotic solvent used experimentally, toluene, does not compete in hydrogen bonding. To perform a conformational search as exhaustive as possible, the amide groups were systematically given opposite orientations, and the branches were oriented to alternatingly position the ester or the amide close to amide hydrogens, to allow hydrogen bonds. A modified version of Dreiding,[69] here called Dreiding** (see ESI†, Figure S9, Table S2), was used as the force field, with atomic charges assigned from the Polymer Consistent Force Field (PCFF),[70, 71] and a long-range interaction cutoff set to 14 Å with a spline width of 3 Å. The dielectric constant was distance-dependent. The dimers were first submitted to molecular mechanics (MM) energy minimizations using the Smart Minimizer algorithm until convergence criteria of 0.001 kcal.mol^{-1} and 0.5 kcal.mol^{-1}.Å^{-1} were reached.

The geometries of the stable dimers were further refined at the Density Functional Theory (DFT) level, using the B3LYP functional and the cc-pVDZ basis set with the GD3BJ empirical dispersion to account for the intermolecular interactions; a rms force of 0.0003 was used as a convergence criterion. With the same DFT method, the IR vibrational frequencies and intensities of the dimers were calculated. The IR spectra were computed based on the calculated vibrational frequencies taking into account a typical 0.97 scaling factor, and a HWHM of 10 cm^{-1}. The calculations were performed using the Gaussian16 package.[72] Full experimental and computed FT-IR spectra for all conformers investigated in this paper are given in Figure S11. Frequencies and dipole strengths of the computed FT-IR spectra are given in Table S4-S14.

Molecular Dynamics (MD) simulations were then performed on two conformations of dimers, the [6 – 6/0] (spiral-type) and [1,1,1,1,1,1 – 6/0] (crossed-type) conformers, in the canonical (N,V,T) ensemble, using similar parameters as for MM. The Nose[73] thermal bath coupling was used to maintain the temperature at 298 K, with a coupling constant of 0.01, and the Verlet[74] velocity algorithm was used to integrate the equations of motion during 1 µs, with a 1-fs time step. Analyses were performed on 20000 structures saved during the MD run. Molecular dynamics simulations were also performed on the two experimental crystalline structures of **BTA Gly$^{t\text{-}Bu}$** discussed in the paper (details in the ESI†). The simulations show that the cell parameters are well reproduced (Table S3). The organization of the molecules and the network of hydrogen bonds (Figure S10) are also maintained throughout the dynamics, thus showing no competition between amides and esters for hydrogen bonding. These observations support our view that Dreiding** is appropriate to model the **BTA Gly** derivatives.

Results

Nomenclature of the different conformations

The dimeric structures mentioned throughout this paper adopt conformations which can be sorted adequately by comparing: i) the relative orientation of the consecutive amide carbonyls, as seen when the dimer is observed perpendicularly to the aromatic rings and ii) the number of intra-dimer hydrogen bonds with ester carbonyls on one hand, and with amide carbonyls on the other hand, as acceptors (Chart 1f). To label each possible conformation of the dimers, we used the following convention [*x* – *y*], for which *x* indicates a series of values (separated by a comma), each one corresponding to the number of consecutive amide carbonyls oriented in the same direction (the sum of these numbers is thus six, i.e., the total number of HB carbonyls in a dimer) and *y* is related to the number of ester and amide carbonyls acting as hydrogen bond acceptors, respectively (ester/amide). The present notation does not discern the potential enantiomeric forms of the dimers. The crossed-type dimeric structure represented in Chart 1d is labelled as [1,1,1,1,1,1 – 6/0], since all consecutive carbonyls adopt alternating orientation and the 6 ester carbonyls are engaged in hydrogen bonds. Similarly, the spiral-type dimeric structure in Chart 1e is labelled as [6 – 6/0], since all the six amide carbonyls are

View Article Online
DOI: 10.1039/D0CP06128J

ARTICLE

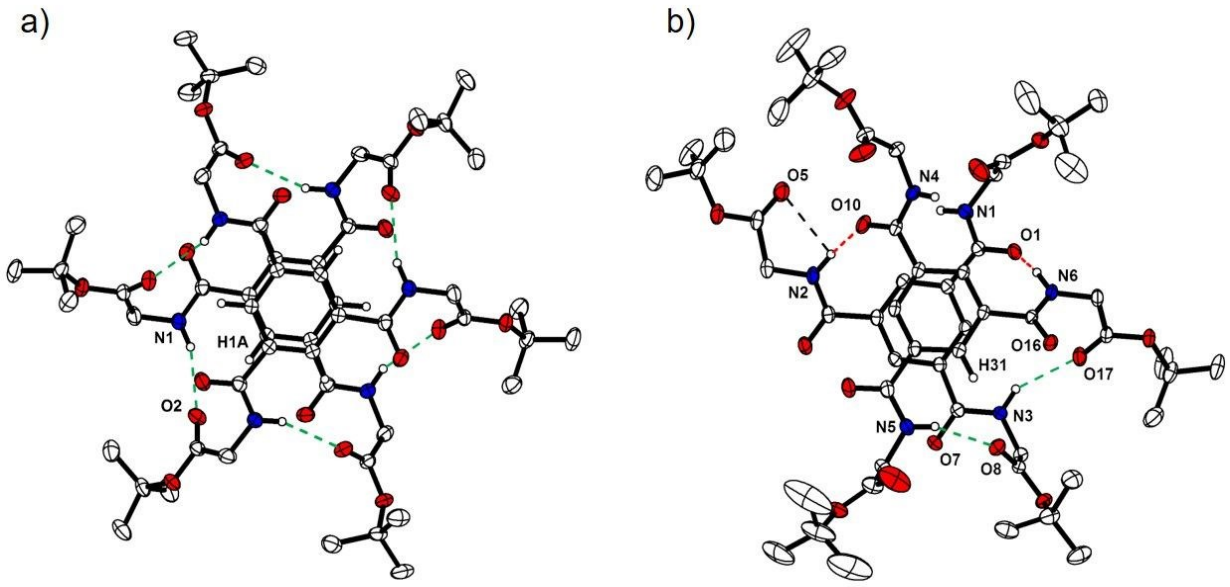

Figure 1 X-ray structures of **BTA Gly$^{t\text{-Bu}}$**. (a) ORTEP representation of the spiral-type dimeric structure ([6 – 6/0] conformation). Selected distances (Å): H1···O2: 2.174(1), H1A···O2: 2.550(1). Selected angles (°): N1-H1···O2: 159.77(8), C1-H1A···O2: 155.99(7). b) ORTEP representation of the dissymmetric dimeric structure ([4,2 – 2/2] conformation). Selected distances (Å): H2···O10: 2.168(2), H2···O5: 2.472(2), H6···O1: 2.140(2), H3···O17: 2.264(2), H5···O8: 2.064(2), H31···O8: 2.455(2). Selected angles (°): N2-H2···O10: 140.62(12), N2-H2···O5: 98.17(12), N6-H6···O1: 146.32(12), N3-H3···O17: 147.83(12), N5-H5···O8: 161.45(13), C31-H31···O8: 146.13(12). Hydrogen atoms that are not involved in hydrogen bonds are omitted for clarity. The green (red) dashed lines correspond to H-bonds involving the ester (amide) C=O groups. The hydrogen bond of the C5 ring involving O5 is shown as a black dashed line.

oriented in the same way and, here again, the 6 ester carbonyls are engaged in hydrogen bonds.

Design, synthesis and crystallization of BTA Gly$^{t\text{-Bu}}$

It is well established that the structure of hydrogen-bonded assemblies in solution might drastically differ from that of the solid state. It is particularly remarkable for ester BTAs since helical stacks have mainly been identified in crystalline, liquid crystalline and gel states but only a small proportion of ester BTAs reported to date actually assemble into stacks in apolar solvents.[58] The single crystal X-ray analysis of **BTA Gly^{Me}** (Chart 1c) reported by Gunnlaugsson and co-workers[61] follows this general picture since the molecules are arranged in a columnar packing with a triple hydrogen bonding network, in conformity with the standard helical structure found for alkyl BTAs and other ester BTAs in crystalline state (Chart 1a). However, we also previously identified ester BTAs that adopt the same hydrogen bond pattern both in the crystalline state and in solution and this proved to be helpful, notably to determine the precise molecular arrangement of the crossed-type dimeric structure.[59] We posited that the bulky *t*-Bu ester groups in **BTA Gly$^{t\text{-Bu}}$** might favour the formation of dimeric structures, which could help to identify the nature of the species present in solution. The reaction between benzene-1,3,5-tricarbonyl trichloride and the *tert*-butyl ester HCl salt of glycine in the presence of triethylamine affords **BTA Gly$^{t\text{-Bu}}$** as a crystalline solid (86% yield, see the ESI†). ^{1}H NMR, ^{13}C{^{1}H} NMR and HRMS analyses confirm the structure and purity of the title compound (ESI†). Single crystals were obtained by slow diffusion of hexane into a DCM solution of **BTA Gly$^{t\text{-Bu}}$** (layering technique). Two distinct types of single crystals formed under these conditions, and were subjected to X-ray diffraction analysis.

Spiral-type dimeric structure of BTA Gly$^{t\text{-Bu}}$ ([6 – 6/0] conformation)

The first type of crystals was refined in the cubic space group *Pa*-3 with one third of the title compound in the asymmetric unit. Symmetry operators (C_3 axis and inversion center) generate a S_6-symmetrical hydrogen-bonded dimer (Figure 1a), *i.e.* a spiral-type [6 – 6/0] structure closely related to that formed by **acid BTA** described in Chart 1e. The distance and angles relative to HB in the dimeric structures of **BTA Gly$^{t\text{-Bu}}$** and of **acid BTA**,[64] as well as in the stacks of **BTA Gly^{Me}**,[61] are compared in Table S1. The amide N–H are exclusively bonded to ester carbonyls (2.174(1) Å), the latter being also engaged in a weaker hydrogen-bonding interaction with aromatic C–H (2.550(1) Å). Because of symmetry operations, the aromatic rings are parallel and co-aligned, *i.e.*, π-π stacked. The inter-centroid distance is slightly lower than that in **acid BTA**: (3.558(2) Å versus 3.660(3) Å). The major difference between the two crystalline structures actually comes from the nature of the interactions between the dimers: bridged via hydrogen bonds to water molecules present in the crystal lattice for **acid BTA**, versus weak *t*-Bu/*t*-Bu and *t*-Bu/C=O contacts for **BTA Gly$^{t\text{-Bu}}$**.

View Article Online
DOI: 10.1039/D0CP06128J

ARTICLE

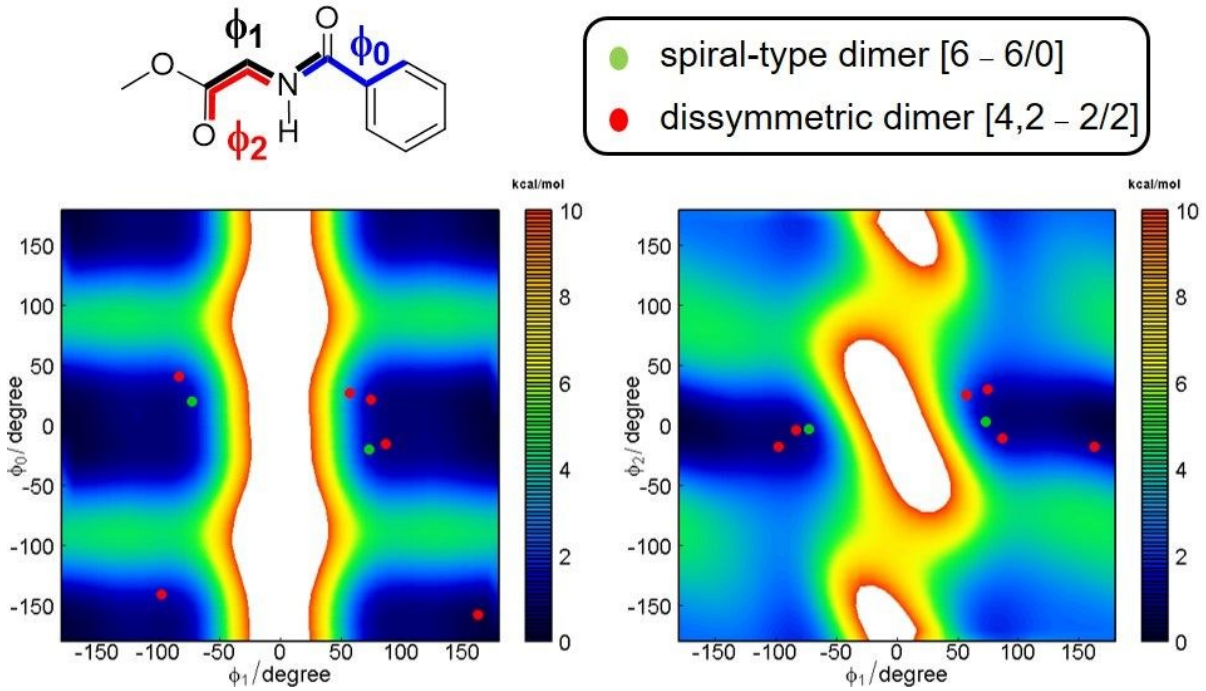

Figure 2 Dreiding** energy maps of an isolated BTA branch as a function of ϕ1-ϕ0 and ϕ1-ϕ2. The angle ϕ0 defines the orientation of the amide with respect to the core; ϕ1 and ϕ2 define the orientation of the ester moiety with respect to the amide. The conformations of the **BTA Gly$^{t\text{-}Bu}$** branches found in the crystalline structures are represented as dots: green dots for the spiral dimer, red dots for the dissymmetric one. The white areas correspond to potential energies >10 kcal.mol^{-1} with respect to the minimum, and thus represent forbidden conformations due to extremely high steric hindrance.

Dissymmetric dimeric structure of BTA Gly$^{t\text{-}Bu}$ ([4,2 – 2/2] conformation)

The data obtained for the second type of crystals were solved and the structural model refined in the monoclinic space group $P2_1/c$. The asymmetric unit contains two molecules of the title compound. Intramolecular hydrogen bonding interactions and π–π stacking of the BTA rings (Figure 1b) generate a dimeric structure (Figure 1b). Angles and distances (caption of Figure 1 and Table S1) are consistent with four classical hydrogen bonds, which involve two amide carbonyls and two ester carbonyls as HB acceptors. Non-classical hydrogen bonding interactions between H2 and O5 (generating a C5 hydrogen bond ring)[75] and between H31 and O8 may also contribute (albeit far more modestly) to the stabilization of the dimers. The hydrogen bond between H5 and ester oxygen O8 (2.064(2) Å) actually appears to be the strongest HB interaction within this dimeric structure, since HBs involving the amide groups and the other ester carbonyl are longer (> 2.14 Å) and significantly distorted (N–H···O angle < 147° *versus* 162° for N5–H5···O8). The aromatic rings are stacked (3.471(3) Å) but experience a deviation from their ideal parallel arrangement (tilt of 6.3°, offset of 0.5 Å). The dissymmetric nature of the dimeric structure is further revealed by the fact that all amide groups are twisted from the plane of the aromatic rings with significantly different angles (Table S1). Unlike the spiral-type dimers, additional hydrogen bond interactions are also established with neighbouring dimers. Amide H4 and H1, and amide O16 and O7, are not involved in HB within the dimeric structure but engage in HB interactions with three other dimers (Figure S1). These inter-dimer HB are stronger than the aforementioned intra-dimer HB, with H···O distances of about 2.027 Å, and N-H···O angles close to 170°. Notably, H4 and O16 atoms connect reciprocally two enantiomeric dimers, thus generating a centrosymmetric $R_2^2(16)$ hydrogen-bonded ring (Figure S1b). In total, four HB are shared between a dimer and its neighbours, thus corresponding energetically to two HB per dimer. It yields a total of four intra-dimer HB and the equivalent of two inter-dimer HB, *i.e.*, the six strong HB donors are involved in the hydrogen bond network. The relative orientation of the amide carbonyls and the hydrogen pattern indicates that this dimer adopts an unanticipated [4,2 – 2/2] conformation (the two inter-dimer HB are not indicated in our nomenclature), with no symmetry operations relating the two molecules.

Energy maps of the dimers in their crystalline structures

The fact that both crystalline structures contain the same molecule as dimers but with strikingly different types of conformation and HB interactions prompted us to probe their side chain conformations, by localizing them on a potential energy map (Figure 2). In both

View Article Online
DOI: 10.1039/D0CP06128J

ARTICLE

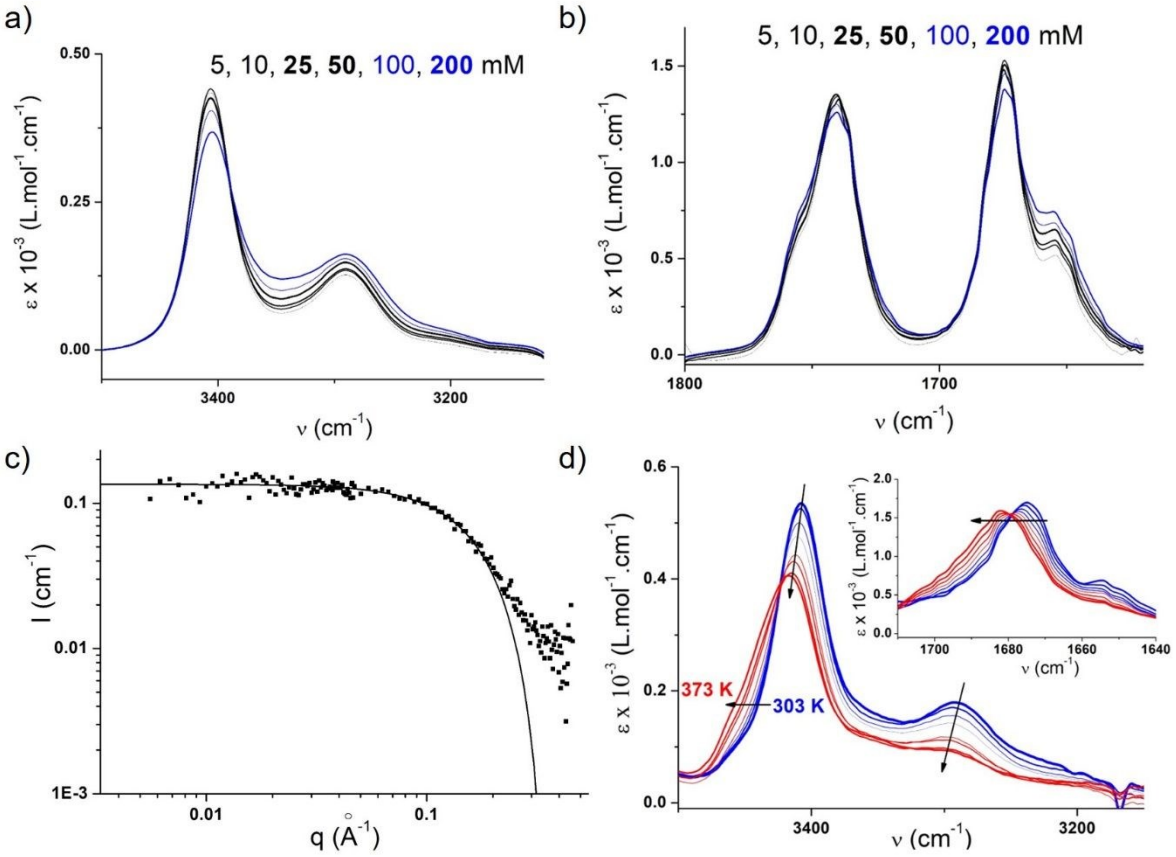

Figure 3 Self-assembly properties of **BTA Gly**. a) FT-IR analysis of **BTA Gly** in toluene (5 mM – 200 mM, 293 K). Zoom of the N–H region. b) Zoom of the C=O region (ester and amide I). c) SANS analysis of **BTA Gly** in C_7D_8 (20.0 g.L^{-1}, 22.4 mM, 293 K). d) Variable-temperature FT-IR analysis of **BTA Gly** in toluene (1.0 mM) between 303 K and 373 K (heating rate= 1 K.min^{-1}).

crystalline structures, the conformations of the side chains (the green and red dots) are all located in potential wells, very close in energy (0-3 kcal.mol^{-1}) to the bottom of the well, showing that the HB formation distorts the branches from their preferential orientation, but with a small energy cost with respect to the energy gained by assembling the molecules (the energy gained by forming such type of HB is typically on the order of 5-10 kcal.mol^{-1}).[76, 77] The fact that different locations of the potential energy valleys are compatible with a complete HB network suggests that diverse relative orientations of the ester and amide groups could be tolerated, leading to dimeric structures that dramatically differ by their hydrogen bonded pattern and their symmetry. Subsequently, we examine what would be the dominant structure in the absence of any packing effects, *i.e.* in solution.

Aggregation number of BTA Gly$^{t\text{-Bu}}$ and BTA Gly assemblies in solution

The good solubility of **BTA Gly** in apolar solvents allows us to conduct scattering and spectroscopic studies in a large range of concentrations and temperatures. Toluene was selected as a solvent, instead of cyclohexane in our previous studies,[58] to favour the formation of discrete species. FT-IR analyses of **BTA Gly** between 5 mM and 200 mM do not show any dramatic change in the intensity and frequency of the bands associated to N–H (Figure 3a) and C=O (Figure 3b) vibrations, indicating that discrete species are prominent over this whole concentration range (see below for the assignment). The increased intensity and broadening of the band at *ca.* 3300 cm^{-1} likely arises from some aggregation between these discrete species, but this aggregation is marginal up to 50 mM. The alkyl ester groups obviously play a role in the packing arrangement of **BTA Gly$^{t\text{-Bu}}$** monomers in the crystalline state but solvation is expected to reduce their influence. This is demonstrated in the present case by the fact that **BTA Gly** and **BTA Gly$^{t\text{-Bu}}$** exhibit virtually identical FT-IR signatures (Figure S2a), thus corroborating that these monomers assemble into similar structures in solution. The dimeric nature of these species is confirmed by SANS analysis of a 20 g.L^{-1} solution of **BTA Gly** in C_7D_8. The scattering intensity at low and intermediate q values is perfectly fitted with a model for spherical objects having 1.9 times

View Article Online
DOI: 10.1039/D0CP06128J

ARTICLE

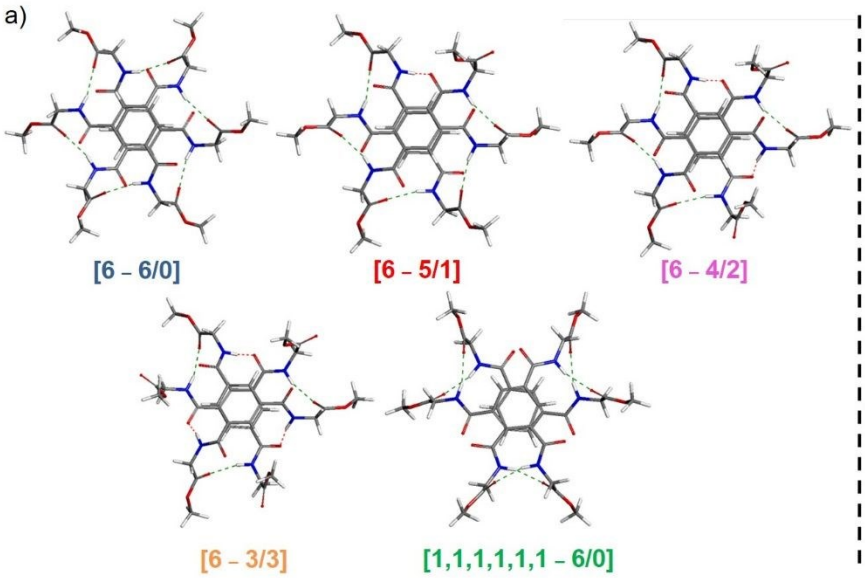

b)

Conformation	Relative energy (kcal.mol^{-1})
[6 – 6/0]	1.7
[6 – 5/1]	0.6
[6 – 4/2]	0.0
[6 – 3/3]	0.4
[5,1 – 5/1]	4.2
[4,2 – 4/2]	7.0
[3,3 – 4/2]	6.8
[3,1,1,1 – 5/1]	4.4
[2,2,1,1 – 5/1]	9.6
[1,1,1,1,1,1 – 6/0]	1.2

Figure 4 a) Selected conformations of **BTA Gly^{Me}** dimers optimized at the B3LYP-GD3BJ/cc-pVDZ level. b) Relative potential energies of the dimeric structures computed in this study. The energies of the selected conformations are highlighted in the Table. See Figure S4 for the other conformations.

the molar mass of **BTA Gly** and a radius of 12.7 Å (Figure 3c). ESI-HRMS analyses of **BTA Gly** (Figure S2b) and **BTA Gly$^{t\text{-}Bu}$** (Figure S2c) also show signals corresponding to dimeric species that are more intense than those corresponding to monomers. Finally, the influence of the temperature on the stability of the dimers was probed by FT-IR analysis (Figure 3d). The gradual shifts of N–H and C=O bands towards higher frequencies indicate that the proportion of free N–H increases with temperature. Yet full disruption of the dimers into monomers is not achieved even at the highest investigated temperature (373 K). The possibility of establishing up to six hydrogen bonds between **BTA Gly** molecules likely explains the remarkable stability of the dimeric species. Even though the aforementioned analyses ascertain the dimeric nature of the species formed by **BTA Gly** in solution, the determination of the nature of the HB network is obscured by the complexity of the FT-IR spectrum (Figures 3a and 3b). Indeed, the observation of several bands in the N–H and amide C=O regions, as well as a shoulder in the ester C=O band, seems to indicate that several types of acceptors are involved in these hydrogen bonded dimers (*vide infra*). Likewise, the FT-IR signature of the discrete dimers formed by **BTA Gly** in toluene is drastically different to from that of the spiral-type and dissymmetric dimers formed by **BTA Gly$^{t\text{-}Bu}$** in the crystalline state (Figure S3). The proportion of amide carbonyl as HB acceptors is notably higher in the dissymmetric dimers than in the dimers present in solution.

Computed structures of BTA Gly^{Me} dimers

The marked difference between the conformations adopted by **BTA Gly$^{t\text{-}Bu}$** in the crystalline state and by **BTA Gly** in solution prompted us to perform a detailed conformational search on **BTA Gly^{Me}** (the dodecyl chain was replaced by a methyl to alleviate the computational cost). The conformations were optimized by means of molecular mechanics (MM) energy minimizations and refined at the B3LYP-GD3BJ/cc-pVDZ level. All these conformations have a complete hydrogen bond network, *i.e.* involving the six amide hydrogens, which is a strong stabilizing factor. They differ by the relative orientation of the amide carbonyls (Chart 1f) and the ratio of ester/amide acceptors involved in HB, which varies between 6/0 and 3/3. As **BTA Gly** exists as discrete dimers in solution, the computed dimers only contain intramolecular HB and consequently no more than 50% of amide groups act as HB acceptors (for geometrical reasons). The energies of all the computed structures are collected in Figure 4b relatively to the most stable conformation. Amongst the computed conformations, those having the lowest potential energies are shown in Figure 4a. They belong to the spiral [6] family, with ester/amide ratios of 6/0, 5/1, 4/2 and 3/3, and to the crossed [1,1,1,1,1,1] family, with an ester/amide ratio of 6/0. These five conformations are close in energy, within 2 kcal.mol^{-1}, and thus should weight in the conformational population of the dimer. Conversely, conformations belonging to the [5,1], [4,2], [3,3], [3,1,1,1] and [2,2,1,1] families are significantly higher in energy (see the computed structures in Figure S4). All these results point to the structural richness of the dimeric structures formed by **BTA Gly**, and raise the possibility that several conformations are co-existing, despite exhibiting different HB networks.

Comparison between computed and experimental FT-IR spectra

This exploration of the conformational landscape of **BTA Gly^{Me}** triggered further investigation aimed at determining

View Article Online
DOI: 10.1039/D0CP06128J

ARTICLE

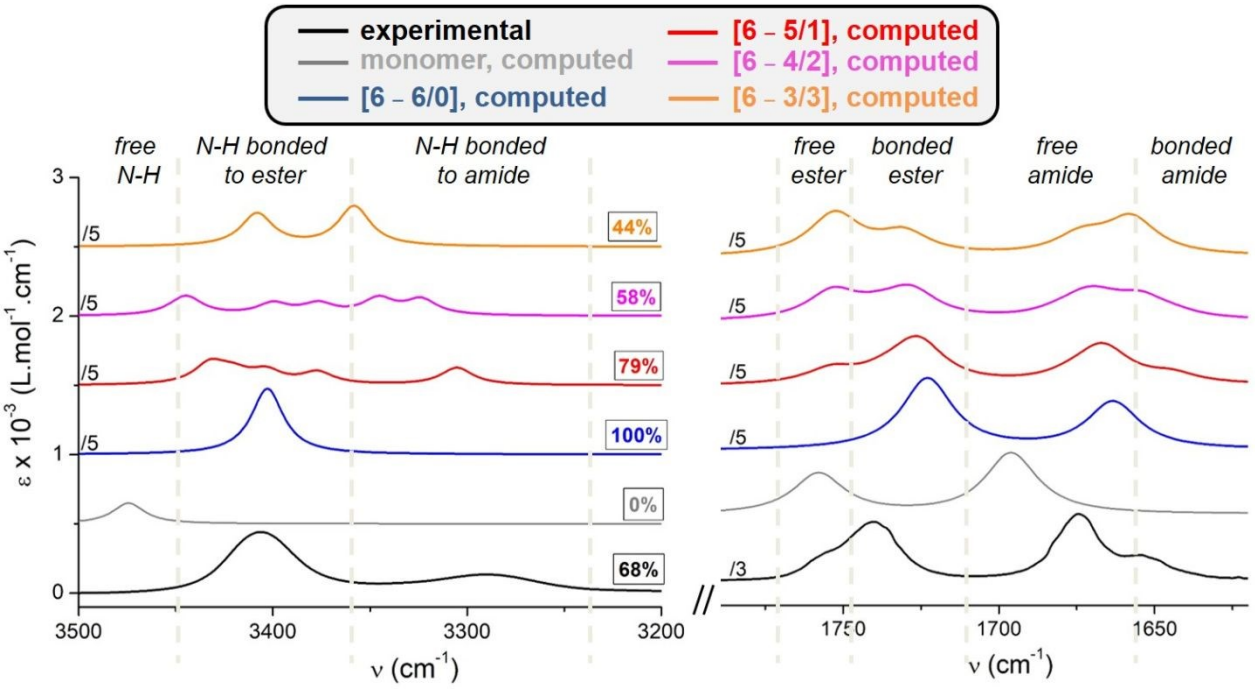

Figure 5 a) Experimental (**BTA Gly**) and computed (**BTA Gly^{Me}**) FT-IR spectra for the monomer and spiral-type conformations. The intensity of certain spectra has been decreased as indicated in order to allow an easier comparison of the experimental and computed FT-IR bands. The percentages correspond, for each spectrum, to the fraction (in area %) of the band(s) corresponding to N–H bonded to ester carbonyls such as f= area of the band(s) corresponding to N–H bonded to ester carbonyls/sum of the areas of the bands corresponding to N–H. These areas have been extracted from the respective deconvoluted spectra (see that of the experimental spectrum in Figure S6b). Accordingly, it was determined that the extinction coefficient associated with the frequency of a N–H bonded to an amide carbonyl is 1.36 times higher than that of a N–H bonded to an ester carbonyl (see the ESI† for more details). It can be thus deduced that conformers of **BTA Gly** dimers contain a 4.5/1.5 ratio of ester/amide as HB acceptors on average (*i.e.* 74±2% of the HB acceptors are ester carbonyls).

experimentally the dominant conformation(s) adopted by the dimers of **BTA Gly**. FT-IR spectroscopy proves to be particularly suitable as the frequency and intensity of the bands associated with HB moieties are particularly sensitive to their environment. We thus calculated the FT-IR spectra of the computed structures of **BTA Gly^{Me}**. First, the spiral-type structures [6 – 6/0] of **BTA Gly^{Me}** (computed) and **BTA Gly$^{t\text{-}Bu}$** (recorded by ATR analysis of single crystals) were compared. Both spectra show FT-IR bands at similar positions, which validates the computational method (Figure S5). Then, the FT-IR spectra of the computed structures were compared to that recorded for **BTA Gly** in toluene (Figures 5 and S6a). As expected, the FT-IR spectra of the spiral-type dimers [6 – 6/0] and crossed-type dimers [1,1,1,1,1,1 – 6/0], which contain only ester carbonyls as HB acceptors, do not conform to the experimental spectrum. Among the computed dimers showing both bonded ester and amide carbonyls, the calculated spectra closest to the experimental one are those of the spiral [6] structures (Figure 5). In the 1600-1800 cm^{-1} region, the FT-IR spectrum of the computed [6 – 5/1] conformer matches best the experimental one. The 3200-3500 cm^{-1} region is more difficult to compare to experiment, as the sensitivity of the N–H vibration to minor structural modifications multiplies the number of peaks in the 5/1 and 4/2 conformations. In dynamic structures, those peaks are expected to be broader and merge, consistent with the two, relatively broad, peaks observed experimentally.

Based on these computed spectra and our previous studies,[57-59] the nature of the bands present in the N–H and C=O (ester and amide I) regions of the FT-IR spectrum of **BTA Gly** (Figures 3 and 5) can be unambiguously assigned as follows: N–H bonded to ester carbonyl (ν_{max}= 3406 cm^{-1}), N–H bonded to amide carbonyl (ν_{max}= 3291 cm^{-1}), free ester carbonyl (ν_{max}= 1757 cm^{-1}), bonded ester carbonyl (ν_{max}= 1740 cm^{-1}), free amide carbonyl (ν_{max}= 1675 cm^{-1}) and bonded amide carbonyl (ν_{max}= 1654 cm^{-1}). A more quantitative determination of the proportion of the HB acceptors was performed by deconvoluting the two bands related to N–H bonded to ester and to amide (Figure S6b). Then, the ratio of the extinction coefficients associated with these N–H stretching frequencies was estimated thanks to the computed FT-IR spectra of the [6 – 5/1], [6 – 4/2] and [6 – 3/3] conformers of **BTA Gly^{Me}** dimers (Figure 5 and ESI†). By assuming that all the N–H are bonded, we found a 4.5/1.5 ester/amide ratio for the HB acceptors in

View Article Online
DOI: 10.1039/D0CP06128J

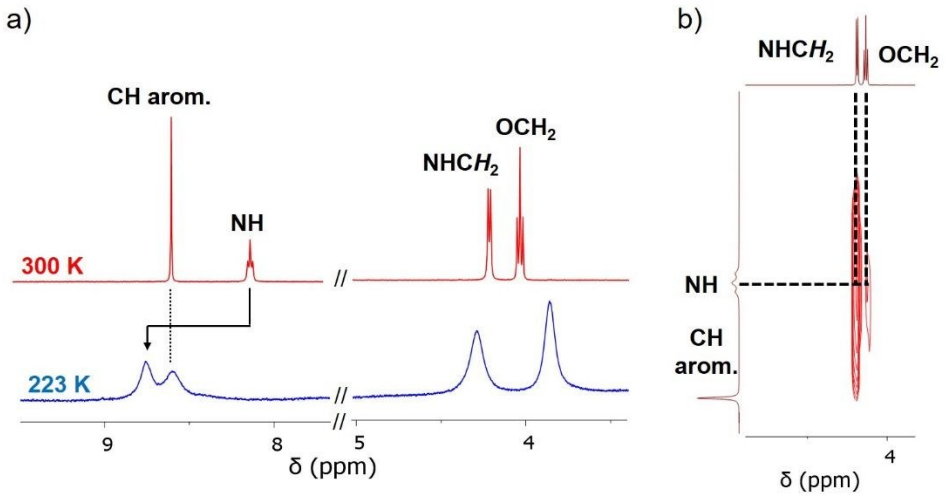

Figure 6 Probing the dynamics of the HB network in **BTA Gly** dimers by NMR analysis. a) ^{1}H NMR analysis of **BTA Gly** (10 mM, C_7D_8) at 300 K and 223 K. Zoom on the region corresponding to the indicated hydrogens. b) NOESY analysis of **BTA Gly** (10 mM, C_7D_8) at 300 K. Zoom on the region related to amide N−H and aromatic C−H.

the discrete dimers formed by **BTA Gly** which translates into 74±2% of the HB acceptors being ester carbonyls. This value is consistent with the fact that none of the computed FT-IR spectra perfectly matches the experimental one and indicates that several conformations of **BTA Gly** dimers actually coexist in solution. The spiral-type dimers are likely to be the dominant species according to this FT-IR study and the aforementioned computed potential energies.

Characterization of BTA Gly dimers by NMR

1D and 2D NMR analyses were conducted in order to gain more information about the nature of the conformations adopted by **BTA Gly** dimers. The ^{1}H NMR spectrum of **BTA Gly** in C_7D_8 is remarkably simple since a single set of signals is observed for each chemical group, *e.g.* a singlet for aromatic C−H and a triplet for amide N−H (Figure 6a). NOESY analysis in C_7D_8 reveals no specific dipolar coupling for aromatic C−H (Figure 6b). This is a particularly striking point since an unambiguous NOE contact was detected between aromatic C−H and the hydrogen atom attached to the amide α carbon in a previously investigated crossed-type dimer.[59] The absence of dipolar coupling surmises that reciprocal hydrogen bonds between the amide N−H and the ester carbonyls of two BTA arms, as observed in crossed-type dimers, are likely not present in **BTA Gly** dimers. This thus infers that crossed-type dimers and other conformations embedding such type of crossed HB pattern do not contribute significantly to the population of **BTA Gly** dimers. Conversely, amide hydrogens exhibit a scalar coupling with their adjacent methylene groups (NCH_2) as well as a more remarkable dipolar interaction with the most deshielded methylene groups of the dodecyl side chain (OCH_2). This indicates that the amide N−H of one BTA molecule and the OCH_2 group of the other BTA molecule are in a relatively close contact within **BTA Gly** dimers. The dynamic nature of the dimers was subsequently probed by performing a ^{1}H NMR analysis at 223 K. Upon lowering the temperature, the equivalent amide N−H are significantly downfield shifted, as a probable consequence of the strengthening of the HB within the dimeric structures. A clear broadening of all NMR signals also occurs, meaning that the chemical exchange is becoming slower at this temperature. However, the dynamic exchange at work in this system appears too rapid on the NMR timescale and the slow exchange regime with distinguishable hydrogen environments cannot be reached at 223 K.

Exchange dynamics of the HB network probed by Molecular Dynamics simulations

In order to better understand the dynamics of the hydrogen bond network in **BTA Gly** dimers, MD calculations were performed on **BTA Gly^{Me}**. The various conformations are sorted according to their family ([6], [5,1], [4,2], [3,1,1,1], [2,2,1,1] and [1,1,1,1,1,1]) during the simulation (Figure 7a) whilst the interconversion between the nature of the HB acceptors for the spiral [6] dimers will be visualized under the form of the energy map shown in Figure 7b. During the 1 μs-long MD simulations (Figure 7a), the complete HB network is maintained, though different organizations of the branches occur. Starting from a [1,1,1,1,1,1] conformation, the dimer reorganizes into a spiral [6] by rotating one branch at a time (to avoid a too high energy penalty), following the general sequence [1,1,1,1,1,1] to [3,1,1,1], then to [5,1], then to [6], though other intermediate families also appear during the reorganization. During the rest of the MD simulation, the spiral [6] dimer-family clearly dominates, with sporadic occurrence of other dimer-families, such as those species close to the spiral one, *i.e.* the [5,1] and [4,2] dimers. Interconversion between spiral-type dimers likely needs these intermediates to avoid a too high energy penalty, following various sequences such as: [6], [5,1], [4,2], [2,2,1,1], [2,4], [1,5], and [6]. Similar results were obtained in the MD simulations performed with a [6] conformation as the starting point (Figure S7). Upon considering the spiral-type dimer, a fast exchange occurs between ester and amide in competition for HB during the

View Article Online
DOI: 10.1039/D0CP06128J

ARTICLE

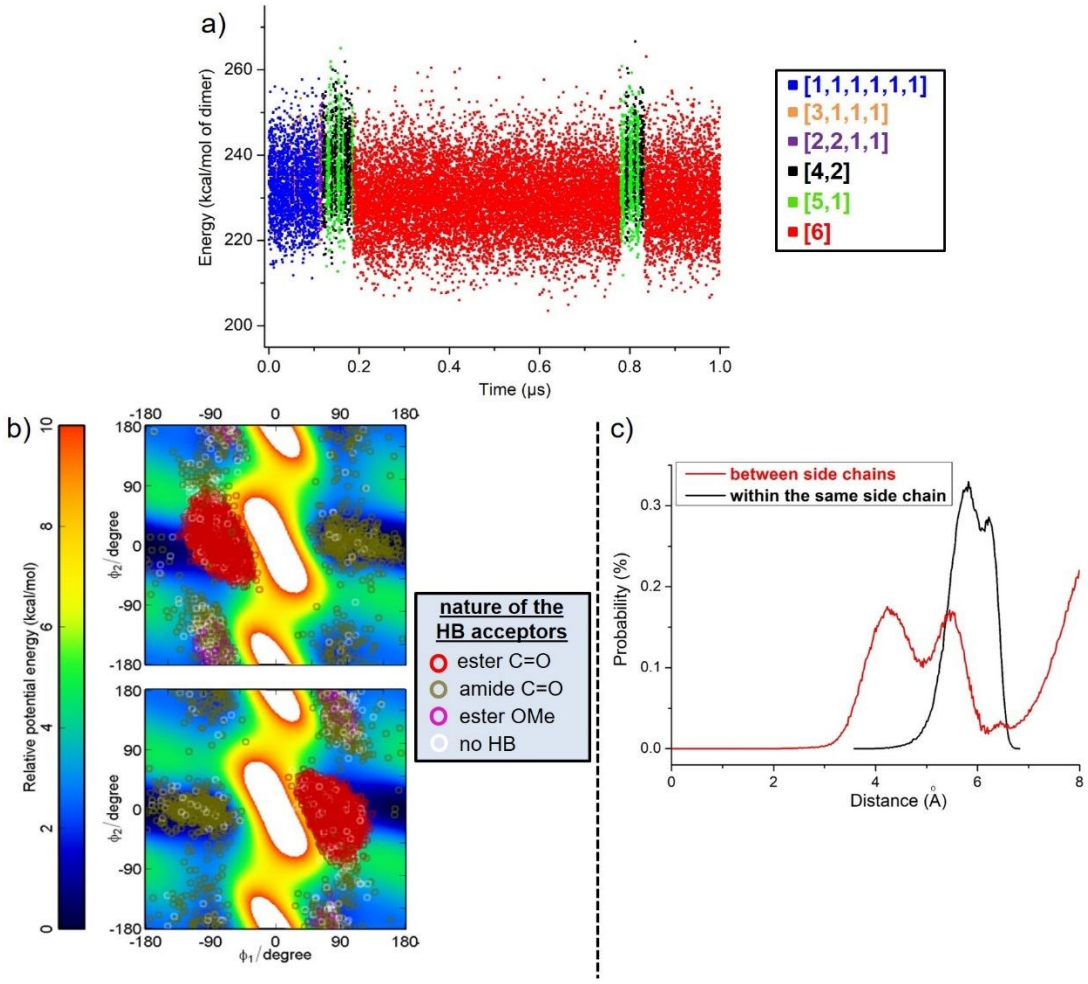

Figure 7 a) MD trajectory of a **BTA Gly^{Me}** dimer of the type [1,1,1,1,1,1 – 6/0] as starting conformation. b) Dreiding** energy maps of the branches of one BTA molecule (top) and of the other BTA molecule (bottom) as function of ϕ1 and ϕ2. The conformations of the **BTA Gly^{Me}** branches of the spiral [6] structures observed during the MD simulations are represented as open dots with a colour depending on the nature of the HB acceptor. c) Distribution of the H···H distance between the N–H and the methyl ester groups, as observed in the MD simulations.

simulations. Each branch sequentially occupies all the potential energy valleys of the ϕ1-ϕ2 energy map (Figure 7b). It appears clearly that the dark yellow dots (corresponding to conformations involving H-bonded amides) populate large parts of the map whereas the red dots (corresponding to H-bonded esters) are localized in a single valley. This reflects the fact that when a branch is bonded via its amide group as acceptor, it remains more flexible than when it is bonded via its ester. As the ϕ1-ϕ2 angles define the orientation of the ester, the ester chain is constrained in a given orientation when H-bonded, and rotates more easily when not H-bonded, *i.e.* when replaced by the amide group as HB acceptor. Interestingly, the short H···H distance of 4.3 Å between the N–H and OCH_3 groups of two different BTA arms corresponds to branches hydrogen bonded through ester carbonyl (Figures 7c and S8). This proximity is consistent with a NOE contact between the N–H and OCH_2 protons observed in the NMR analysis of **BTA Gly** (Figure 6b). This result infers that the majority of the branches present in the vast range of conformations adopted by **BTA Gly** dimers have an orientation similar to that present in the spiral-type conformer [6 – 6/0]. This observation is in agreement with both spiral-type dimers being the major species and 75% of HB acceptors being ester carbonyls, as deduced from the aforementioned spectroscopic data.

Discussion

The BTA monomers derived from different glycine alkyl esters studied in this paper contain amide functions that are relatively flexible compared to derivatives of other amino-acids. Several consequences of this flexibility could have been

View Article Online
DOI: 10.1039/D0CP06128J

ARTICLE

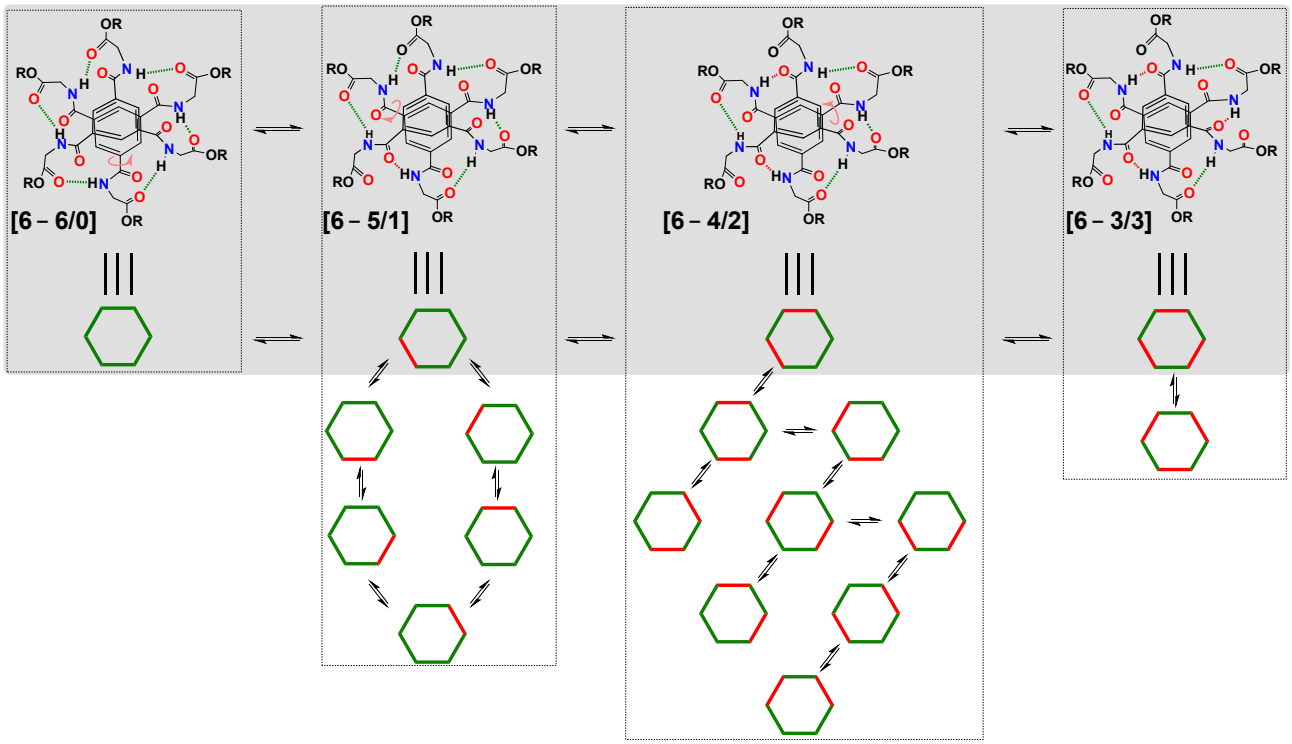

Figure 8 Proposed model for the fluxional HB network operating in **BTA Gly** dimers. The exchange cycle makes all protons in **BTA Gly** magnetically equivalent on the NMR timescale. Only one conformer for each type of spiral-type dimers is drawn. The other conformers are schematized as hexagons in which the sides represent the hydrogen bonds (as red and green lines for amide and ester HB acceptors, respectively). By convention, only species that can be interconverted by rotation of a single BTA branch are shown to be in equilibrium.

(wrongly) anticipated: i) no aggregation, ii) the formation of ill-defined objects or iii) assemblies with different aggregation numbers. The flexibility of the monomer backbone is considered as an element of design for assemblies exhibiting "polymorphic structures", *i.e.,* structural changes as a function of the experimental conditions.[28] Like previously investigated ester BTA assemblies,[57-59] dimers are the privileged species formed upon assembly of **BTA Gly** monomers. However, the intrinsic flexibility of these monomers leads to the following properties: i) polymorphism in the crystalline state gives rise to dimeric structures that differ by their hydrogen bond pattern, including one dissymmetric structure involving both ester and amide functions as HB acceptors, ii) several conformations of **BTA Gly** dimers coexist in solution, and are in dynamic equilibrium.

Our combined experimental and computational studies allow gaining more information about the nature of the major conformations present in solution. FT-IR spectroscopy reveals that 74±2% of the HB acceptors are ester carbonyls whilst 26±2% are amide carbonyls. Likewise, NOESY analysis is consistent with the molecular arrangement present in spiral-type dimers, and not with that found in crossed-type dimers, *i.e.* that most of the BTA branches are connected by a single hydrogen bond. These observations, combined with the relative energies of the computed structures of **BTA Gly^{Me}** dimers, suggest that spiral-type dimers are the dominant structures. The spiral-type dimers, even though they differ by the ratio of ester and amide carbonyls as HB acceptors, have similar potential energies. The multiplicity, *i.e.* the number of different conformations, of the spiral-type dimers [6 – 6/0], [6 – 5/1], [6 – 4/2] and [6 – 3/3] are 1, 6, 9 and 2, respectively (Figure 8), not counting enantiomers. Considering as a first approximation that all these conformations have the same energies yields 72% of HB acceptors being ester carbonyls, which is in good agreement with the value determined experimentally.[78]

Exchange rates between monomers of BTA helical assemblies was previously found to occur on the time scale of seconds,[38, 79] at the fastest.[41] The rapid hydrogen bond reshuffling that occurs in solution between the different conformers of **BTA Gly^{Me}** dimers appears to occur at a much higher rate in the present case. Hydrogen bond exchange occurs between

monomers belonging to the same structure and thus, below the ns timescale for the ester-amide competition, according to MD. This fluxional nature of **BTA Gly^{Me}** dimers is attributed to the vicinity of the ester and amide groups, which allows them to be simultaneously close to the amide hydrogens, and favors a smooth transition of HB from one acceptor to the other. Conformational changes from the spiral family to another family are less frequent, as at least a full BTA branch has to break HB to rotate by about 180°. Such changes are rare during the 1-μs long MD simulations, and the persistence time of the non-spiral families (*e.g.* [5,1] and [4,2] structures) is only of a few ns. Conversely, the spiral [6] family can persist for hundreds of ns, demonstrating the higher kinetic stability of this family of conformers.

The ester-amide competition occurring in these HB dimers exhibits some analogy with the reports of proton transfer and hydrogen-bond exchange in intermolecular acid-base interactions.[80] Proton transfers and motions in neutral[80, 81] or charged[80, 82] hydrogen-bonded complexes are fast in solution and NMR allows characterizing averaged HB geometries. Conversely, UV-Vis absorption[82] and FT-IR[83] analyses were exploited to detect the different hydrogen bonding configurations present in these rapid equilibria. A similar observation can be made in the present system. The interconversion between all **BTA Gly** conformers in equilibrium is rapid on the NMR analysis, the timescale of which only permits to probe an averaged geometry accounting for all the conformers in rapid exchange. However, FT-IR analysis provides a snapshot of the dimeric structures present in equilibrium thus allowing to detect the presence of dimers with lower symmetry.

A model that accounts for both FT-IR and NMR analyses is presented in Figure 8, where we consider that all spiral-type dimers are in equilibrium through low energy changes of ϕ0, ϕ1, and ϕ2 (allowed by a flat energy landscape for a large range of torsion values, see Figure 2). The weighed distribution of the conformers is not known but it can be expected that each conformer contributes more or less equally to the overall population given their similar potential energies. Among these structures, the conformation with no H-bonded amide, [6 – 6/0], is of higher symmetry. As each arm can behave similarly to the others, one can envisage six different conformations when one amide acceptor is H-bonded ([6 – 5/1]), nine with two amide acceptors ([6 – 4/2]), and two with three amide acceptors ([6 – 3/3]). However, as the conformational changes are fast, on average all N–H protons are expected to experience the same environment, thus appearing as magnetically equivalent on the NMR timescale. Even though this model provides a good illustration of the hydrogen bond dynamic exchange at work in **BTA Gly** dimers, it only involves spiral [6] conformers. MM/MD calculations suggest the involvement of other dimer families, but their weight in the population is likely small due to energy penalty or entropy penalty.

Conclusion

View Article Online
DOI: 10.1039/D0CP06128J

Our thorough experimental and computational studies aimed at determining the self-assembly behavior of benzene-1,3,5-tricarboxamide molecules derived from glycine alkyl esters reveal unanticipated features for this class of monomers. Highly symmetric dimeric structures with ester carbonyl as the exclusive HB acceptors are in competition with dimers of lower symmetry in which both ester and amide play the role of acceptors. These assemblies have been characterized both in the crystalline state and in solution. In the latter case, a variety of conformers exhibiting different symmetries appears to be in rapid exchange. Conformers of the spiral-type, *i.e.* with the same relative orientation of the amide carbonyl as seen when the dimer is observed perpendicularly to the aromatic rings, are likely to be the dominant conformers in solution. The fluxional nature of **BTA Gly** dimers can be rationalized by the fact that low-energy changes associated with ϕ0, ϕ1, and ϕ2 torsion angles allow ester and amide to compete for the bonding of the same amide hydrogen. The interconversion rate between all conformers is rapid on the NMR timescale but slow on that of FT-IR, allowing dimers of different symmetries to be detected. These results point out to the importance of using different spectroscopic techniques in order to precisely determine the HB network of dynamic assemblies.

The flexibility of the side-chains present in **BTA Gly** monomers allows a range of energetically close conformations to be accessible in the dimeric state. Such conformations have not been detected in the case of other ester BTA monomers,[57-59, 62] highlighting the richness of the structures accessible by simple modulation of the group connected to the amide α carbon. The co-assembly of monomers of different nature constitutes the next step for the construction of intricate functional supramolecular architectures.

Conflicts of interest

There are no conflicts to declare.

Acknowledgements

This work was supported by the China Scholarship Council (CSC, Ph.D. grant of Y.L.). Jacques Jestin (LLB, Saclay) is acknowledged for assistance with SANS experiments. This manuscript is in honor of the 50 year anniversary of the French Polymer Group (Groupe Français des Polymères - GFP). Research in Mons is supported by Fonds National de la Recherche Scientifique (FNRS) via the Excellence of Science program (2Dto3D project) and Consortium des Equipements de Calcul Intensif (CECI).

References

1. J. M. Lehn, *Angew. Chem. Int. Ed.*, 2013, **52**, 2836-2850.
2. E. Busseron, Y. Ruff, E. Moulin and N. Giuseppone, *Nanoscale*, 2013, **5**, 7098-7140.

3. D. B. Amabilino, D. K. Smith and J. W. Steed, *Chem. Soc. Rev.*, 2017, **46**, 2404-2420.
4. F. Ishiwari, Y. Shoji and T. Fukushima, *Chem. Sci.*, 2018, **9**, 2028-2041.
5. A. R. A. Palmans and E. W. Meijer, *Angew. Chem. Int. Ed.*, 2007, **46**, 8948-8968.
6. C. C. Lee, C. Grenier, E. W. Meijer and A. P. H. J. Schenning, *Chem. Soc. Rev.*, 2009, **38**, 671-683.
7. M. H. Liu, L. Zhang and T. Y. Wang, *Chem. Rev.*, 2015, **115**, 7304-7397.
8. E. Yashima, N. Ousaka, D. Taura, K. Shimomura, T. Ikai and K. Maeda, *Chem. Rev.*, 2016, **116**, 13752-13990.
9. Y. Dorca, J. Matern, G. Fernández and L. Sánchez, *Isr. J. Chem.*, 2019, **59**, 869-880.
10. S. Cantekin, T. F. A. de Greef and A. R. A. Palmans, *Chem. Soc. Rev.*, 2012, **41**, 6125-6137.
11. Y. Matsunaga, N. Miyajima, Y. Nakayasu, S. Sakai and M. Yonenaga, *Bull. Chem. Soc. Jpn.*, 1988, **61**, 207-210.
12. A. Timme, R. Kress, R. Q. Albuquerque and H. W. Schmidt, *Chem. Eur. J.*, 2012, **18**, 8329-8339.
13. D. Wang, Y. Huang, J. Li, L. Xu, M. Chen, J. Tao and L. Li, *Chem. Eur. J.*, 2013, **19**, 685-690.
14. M. P. Lightfoot, F. S. Mair, R. G. Pritchard and J. E. Warren, *Chem. Commun.*, 1999, 1945-1946.
15. M. Kristiansen, P. Smith, H. Chanzy, C. Baerlocher, V. Gramlich, L. McCusker, T. Weber, P. Pattison, M. Blomenhofer and H. W. Schmidt, *Cryst. Growth. Des.* , 1999, **9**, 2556-2558.
16. L. Brunsveld, A. P. H. J. Schenning, M. A. C. Broeren, H. M. Janssen, J. A. J. M. Vekemans and E. W. Meijer, *Chem. Lett.*, 2000, 292-293.
17. M. M. J. Smulders, T. Buffeteau, D. Cavagnat, M. Wolffs, A. P. H. J. Schenning and E. W. Meijer, *Chirality*, 2008, **20**, 1016-1022.
18. P. J. M. Stals, M. M. J. Smulders, R. Martín-Rapún, A. R. A. Palmans and E. W. Meijer, *Chem. Eur. J.*, 2009, **15**, 2071-2080.
19. Y. Nakano, T. Hirose, P. J. M. Stals, E. W. Meijer and A. R. A. Palmans, *Chem. Sci.*, 2012, **3**, 148-155.
20. K. Hanabusa, C. Koto, M. Kimura, H. Shirai and A. Kakehi, *Chem. Lett.*, 1997, 429-430.
21. D. Ogata, T. Shikata and K. Hanabusa, *J. Phys. Chem. B*, 2004, **108**, 15503-15510.
22. T. Shikata, Y. Kuruma, A. Sakamoto and K. Hanabusa, *J. Phys. Chem. B*, 2008, **112**, 16393-16402.
23. P. Besenius, K. P. van den Hout, H. M. H. G. Albers, T. F. A. de Greef, L. L. C. Olijve, T. M. Hermans, B. F. M. de Waal, P. H. H. Bomans, N. A. J. M. Sommerdijk, G. Portale, A. R. A. Palmans, M. H. P. van Genderen, J. A. J. M. Vekemans and E. W. Meijer, *Chem. Eur. J.*, 2011, **17**, 5193-5203.
24. C. M. A. Leenders, L. Albertazzi, T. Mes, M. M. E. Koenigs, A. R. A. Palmans and E. W. Meijer, *Chem. Commun.*, 2013, **49**, 1963-1965.
25. H. Frisch, J. P. Unsleber, D. Lüdeker, M. Peterlechner, G. Brunklaus, M. Waller and P. Besenius, *Angew. Chem. Int . Ed.*, 2013, **52**, 10097-10101.
26. H. Frisch, Y. Nie, S. Raunser and P. Besenius, *Chem. Eur. J.*, 2015, **21**, 3304-3309.
27. M. Garzoni, M. B. Baker, C. M. A. Leenders, I. K. Voets, L. Albertazzi, A. R. A. Palmans, E. W. Meijer and G. M. Pavan, *J. Am. Chem. Soc.*, 2016, **138**, 13985-13995.
28. N. M. Matsumoto, R. P. M. Lafleur, X. Lou, K.-C. Shih, S. P. W. Wijnands, C. Guibert, J. W. A. M. van Rosendaal, I. K. Voets, A. R. A. Palmans, Y. Lin and E. W. Meijer, *J. Am. Chem. Soc.*, 2018, **140**, 13308-13316.
29. T. Klein, F. V. Gruschwitz, S. Rogers, S. Hoeppener, I. Nischang and J. C. Brendel, *J. Colloid. Interf. Sci.*, 2019, **557**, 488-497.
30. S. P. W. Wijnands, W. Engelen, R. P. M. Lafleur, E. W. Meijer and M. Merkx, *Nat. Commun.*, 2018, **9**, doi: 10.1038/s41467-41017-02559-41460.
31. M. A. A. Garcia, E. M. Estirado, L. G. Milroy and L. Brunsveld, *Angew. Chem. Int . Ed.*, 2018, **57**, 4976-4980.
32. E. M. Estirado, A. F. Mason, M. A. A. Garcia, J. C. M. van Hest and L. Brunsveld, *J. Am. Chem. Soc.*, 2020, **142**, 9106-9111.
33. M. de Torres, R. van Hameren, R. J. M. Nolte, A. E. Rowan and J. A. A. W. Elemans, *Chem. Commun.*, 2013, **49**, 10787-10789.
34. M. Raynal, F. Portier, P. W. N. M. van Leeuwen and L. Bouteiller, *J. Am. Chem Soc.*, 2013, **135**, 17687-17690.
35. E. Huerta , B. van Genabeek , B. A. G. Lamers, M. M. E. Koenigs, E. W. Meijer and A. R. A. Palmans, *Chem. Eur. J.*, 2015, **21**, 3682-3690.
36. L. N. Neumann, M. B. Baker, C. M. A. Leenders, I. K. Voets, R. P. M. Lafleur, A. R. A. Palmans and E. W. Meijer, *Org. Biomol. Chem.*, 2015, **13**, 7711-7719.
37. A. Desmarchelier, X. Caumes, M. Raynal, A. Vidal-Ferran, P. W. N. M. van Leeuwen and L. Bouteiller, *J. Am. Chem. Soc.*, 2016, **138**, 4908-4916.
38. J. M. Zimbron, X. Caumes, Y. Li, C. M. Thomas, M. Raynal and L. Bouteiller, *Angew. Chem. Int. Ed.*, 2017, **56**, 14016-14019.
39. Y. Li, X. Caumes, M. Raynal and L. Bouteiller, *Chem. Commun.*, 2019, **55**, 2162-2165.
40. Z. C. Shen, Y. T. Sang, T. Y. Wang, J. Jiang, Y. Meng, Y. Q. Jiang, K. Okuro, T. Aida and M. H. Liu, *Nat. Commun.*, 2019, **10**, doi/10.1038/s41467-41019-11840-41463.
41. Y. Li, A. Hammoud, L. Bouteiller and M. Raynal, *J. Am. Chem. Soc.*, 2020, **142**, 5676-5688.
42. M. A. Martínez-Aguirre, Y. Li, N. Vanthuyne, L. Bouteiller and M. Raynal, *Angew. Chem. Int . Ed.*, 10.1002/anie.202012457.
43. Z. C. Shen, T. Y. Wang, L. Shi, Z. Y. Tang and M. H. Liu, *Chem. Sci.*, 2015, **6**, 4267-4272.
44. O. Kotova, R. Daly, C. M. G. dos Santos, M. Boese, P. E. Kruger, J. J. Boland and T. Gunnlaugsson, *Angew. Chem. Int . Ed.*, 2012, **51**, 7208-7212.
45. B. Adelizzi, N. J. Van Zee, L. N. J. de Windt, A. R. A. Palmans and E. W. Meijer, *J. Am. Chem. Soc.*, 2019, **141**, 6110-6121.
46. E. Weyandt, G. M. ter Huurne, G. Vantomme, A. J. Markvoort, A. R. A. Palmans and E. W. Meijer, *J. Am. Chem. Soc.*, 2020, **142**, 6295-6303.
47. E. Weyandt, M. F. J. Mabesoone, L. N. J. De Windt, E. W. Meijer, A. R. A. Palmans and G. Vantomme, *Org. Mater.*, 2020, **2**, 129-142.
48. G. M. ter Huurne, P. Chidchob, A. G. Long, A. Martinez, A. R. A. Palmans and G. Vantomme, *Chem. Eur. J.*, 2020, *44*, 9964-9970.
49. G. Vantomme, G. M. ter Huurne, C. Kulkarni, H. M. M. ten Eikelder, A. J. Markvoort, A. R. A. Palmans and E. W. Meijer, *J. Am. Chem. Soc.*, 2019, **141**, 18278-18285.
50. M. de Loos, J. H. van Esch, R. M. Kellogg and B. L. Feringa, *Tetrahedron*, 2007, **63**, 7285-7301.
51. M. A. J. Veld, D. Haveman, A. R. A. Palmans and E. W. Meijer, *Soft Matter*, 2011, **7**, 524-531.
52. S. Cantekin, H. M. M. ten Eikelder, A. J. Markvoort, M. A. J. Veld, P. A. Korevaar, M. M. Green, A. R. A. Palmans and E. W. Meijer, *Angew. Chem. Int. Ed.*, 2012, **51**, 6426-6431.
53. P. P. Bose, M. G. B. Drew, A. K. Das and A. Banerjee, *Chem. Commun.*, 2006, 3196-3198.
54. G. Srinivasulu, B. Sridhar, K. R. Kumar, B. Sreedhar, V. Ramesh, R. Srinivas and A. C. Kunwar, *J. Mol. Struct.*, 2011, **1006**, 180-184.
55. P. Jana, A. Paikar, S. Bera, S. K. Maity and D. Haldar, *Org. Lett.*, 2014, **16**, 38-41.
56. A. Paikar, A. Pramanik and D. Haldar, *RSC Advances*, 2015, **5**, 31845-31851.
57. A. Desmarchelier, M. Raynal, P. Brocorens, N. Vanthuyne and L. Bouteiller, *Chem. Commun.*, 2015, **51**, 7397-7400.
58. A. Desmarchelier, B. G. Alvarenga, X. Caumes, L. Dubreucq, C. Troufflard, M. Tessier, N. Vanthuyne, J. Idé, T. Maistriaux, D.

View Article Online
DOI: 10.1039/D0CP06128J

Beljonne, P. Brocorens, R. Lazzaroni, M. Raynal and L. Bouteiller, *Soft Matter*, 2016, **12**, 7824-7838.
59. X. Caumes, A. Baldi, G. Gontard, P. Brocorens, R. Lazzaroni, N. Vanthuyne, C. Troufflard, M. Raynal and L. Bouteiller, *Chem. Commun.*, 2016, **52**, 13369-13372.
60. A. D. Lynes, C. S. Hawes, E. N. Ward, B. Haffner, M. E. Möbius, K. Byrne, W. Schmitt, R. Pal and T. Gunnlaugsson, *CrystEngComm*, 2017, **19**, 1427-1438.
61. A. D. Lynes, C. S. Hawes, K. Byrne, W. Schmitt and T. Gunnlaugsson, *Dalton Trans.*, 2018, **47**, 5259-5268.
62. G. Basuyaux, A. Desmarchelier, G. Gontard, N. Vanthuyne, J. Moussa, H. Amouri, M. Raynal and L. Bouteiller, *Chem. Commun.*, 2019, 8548-8551.
63. K. K. Bejagam, R. C. Remsing, M. L. Klein and S. Balasubramanian, *Phys. Chem. Chem. Phys.*, 2017, **19**, 258-266.
64. B. Gong, C. Zheng and Y. Yan, *J. Chem. Cryst.*, 1999, **29**, 649-652.
65. S. Bera, S. K. Maity and D. Haldar, *CrystEngComm*, 2014, **16**, 4834-4841.
66. L. Calabi, A. Maiocchi, M. Lolli and F. Rebasti Diagnostic imaging contrast agent with improved in-serum relaxivity WO9805625, 1998.
67. G. M. Sheldrick, *Acta Cryst. C*, 2015, **71**, 3-8.
68. BIOVIA, Dassault Systèmes, Biovia Materials Studio, 6.0, San Diego: Dassault Systèmes, 2011.
69. S. L. Mayo, B. D. Olafson and W. A. Goddard, III, *J. Phys. Chem.*, 1990, **94**, 8897.
70. H. Sun, *J. Comput. Chem.*, 1994, **15**, 752.
71. H. Sun, *Macromolecules*, 1995, **28**, 701.
72. M. J. Frisch, *et al.*, Gaussian 16 Revision A.03, Gaussian Inc., Wallingford, CT, USA, 2016.
73. S. Nose, *Mol. Phys.*, 1984, **52**, 255.
74. L. Verlet, *Phys. Rev.*, 1967, **159**, 98.
75. R. W. Newberry and R. T. Raines, *Nat. Chem. Biol.*, 2016, **12**, 1084-1089.
76. C. Liu, D. X. Zhao and Z. Z. Yang, *J. Comput. Chem.*, 2012, **33**, 379-390.
77. Y. Zhou, Z. H. Wang, S. D. Gong, Z. W. Yu and X. Z. Xu, *J. Mol. Struct.*, 2018, **1173**, 321-327.
78. A 70/30 ratio of ester/amide as HB acceptors is obtained if all conformations present in Figure 7b are considered.
79. M. M. J. Smulders, A. P. H. J. Schenning and E. W. Meijer, *J. Am. Chem. Soc.*, 2008, **130**, 606-611.
80. P. M. Tolstoy, P. Schah-Mohammedi, S. N. Smirnov, N. S. Golubev, G. S. Denisov and H. H. Limbach, *J. Am. Chem. Soc.*, 2004, **126**, 5621-5634.
81. V. V. Mulloyarova, I. S. Giba, M. A. Kostin, G. S. Denisov, I. G. Shenderovich and P. M. Tolstoy, *Phys. Chem. Chem. Phys.*, 2018, **20**, 4901-4910.
82. B. Koeppe, P. M. Tolstoy and H. H. Limbach, *J. Am. Chem. Soc.*, 2011, **133**, 7897-7908.
83. B. Koeppe, S. A. Pylaeva, C. Allolio, D. Sebastiani, E. T. J. Nibbering, G. S. Denisov, H. H. Limbach and P. M. Tolstoy, *Phys. Chem. Chem. Phys.*, 2017, **19**, 1010-1028.